

Article

Richardsite, $\text{Zn}_2\text{CuGaS}_4$, A New Gallium-Essential Member of the Stannite Group from the Gem Mines near Merelani, Tanzania

Luca Bindi ¹ and John A. Jaszczak ^{2,*}

¹ Dipartimento di Scienze della Terra, Università di Firenze, Via La Pira 4, I-50121 Firenze, Italy; luca.bindi@unifi.it

² Department of Chemistry, Department of Physics, and the A. E. Seaman Mineral Museum, Michigan Technological University, 1400 Townsend Dr., Houghton, MI 49931-1295, USA

* Correspondence: jaszczak@mtu.edu; Tel. +1-906-487-2255

Received: 22 April 2020; Accepted: 17 May 2020; Published: 20 May 2020

Abstract: The new mineral richardsite occurs as overgrowths of small (50–400 μm) dark gray, disphenoidal crystals with no evident twinning, but epitaxially oriented on wurtzite–sphalerite crystals from the gem mines near Merelani, Lelatema Mountains, Simanjiro District, Manyara Region, Tanzania. Associated minerals also include graphite, diopside, and Ge,Ga-rich wurtzite. It is brittle, dark gray in color, and has a metallic luster. It appears dark bluish gray in reflected plane-polarized light, and is moderately birefractant. It is distinctly anisotropic with violet to light-blue rotation tints with crossed polarizers. Reflectance percentages for R_{\min} and R_{\max} in air at the respective wavelengths are 23.5, 25.0 (471.1 nm); 27.4, 28.9 (548.3 nm); 28.1, 29.4 (586.6 nm); 27.7, 28.9 (652.3 nm). Richardsite does not show pleochroism, internal reflections, or optical indications of growth zonation. Electron microprobe analyses determine an empirical formula, based on 8 apfu, as $(\text{Zn}_{1.975}\text{Cu}_{0.995}\text{Ga}_{0.995}\text{Fe}_{0.025}\text{Mn}_{0.010}\text{Ge}_{0.005}\text{Sn}_{0.005})_{\Sigma 4.010}\text{S}_{3.990}$, while its simplified formula is $(\text{Zn,Cu})_2(\text{Cu,Fe,Mn})(\text{Ga,Ge,Sn})\text{S}_4$, and the ideal formula is $\text{Zn}_2\text{CuGaS}_4$. The crystal structure of richardsite was investigated using single-crystal and powder X-ray diffraction. It is tetragonal, with $a = 5.3626(2)$ Å, $c = 10.5873(5)$ Å, $V = 304.46(2)$ Å³, $Z = 2$, and a calculated density of 4.278 g·cm^{−3}. The four most intense X-ray powder diffraction lines [d in Å (I/I_0)] are 3.084 (100); 1.882 (40); 1.989 (20); 1.614 (20). The refined crystal structure ($R1 = 0.0284$ for 655 reflections) and obtained chemical formula indicate that richardsite is a new member of the stannite group with space group $I\bar{4}2m$. Its structure consists of a *ccp* array of sulfur atoms tetrahedrally bonded with metal atoms occupying one-half of the *ccp* tetrahedral voids. The ordering of the metal atoms leads to a sphalerite(sph)-derivative tetragonal unit-cell, with $a \approx a_{\text{sph}}$ and $c \approx 2a_{\text{sph}}$. The packing of S atoms slightly deviates from the ideal, mainly due to the presence of Ga. Using 632.8-nm wavelength laser excitation, the most intense Raman response is a narrow peak at 309 cm^{−1}, with other relatively strong bands at 276, 350, and 366 cm^{−1}, and broader and weaker bands at 172, 676, and 722 cm^{−1}. Richardsite is named in honor of Dr. R. Peter Richards in recognition of his extensive research and writing on topics related to understanding the genesis of the morphology of minerals. Its status as a new mineral and its name have been approved by the Commission of New Minerals, Nomenclature and Classification of the International Mineralogical Association (No. 2019-136).

Keywords: richardsite; stannite group; gallium; sulfide; Merelani tanzanite deposit; Tanzania

1. Introduction

In addition to tanzanite, the blue-purple gem variety of zoisite that is famous from the region, the gem mines near Merelani, Lelatema Mountains, Simanjiro District, Manyara Region, Tanzania, are host to several other unusually well-crystallized minerals, including tsavorite, the green gem variety of grossular, diopside, prehnite, fluorapatite, and even graphite [1–5]. The mines are also host to well-formed and uncommonly large crystals of pyrite, alabandite, and wurtzite as well as several rare sulfides, including clausthalite (PbSe), germanocolusite ($\text{Cu}_{13}\text{VGe}_3\text{S}_{16}$), and merelaniite ($\text{Mo}_4\text{Pb}_4\text{VSbS}_{15}$) [5–7]. A detailed study of the chemistry of intergrown sphalerite and wurtzite, which included samples from the Merelani mines and from the Animas-Chocaya Mine complex, Quechisla district, Bolivia, was recently published [8]. The Merelani sphalerite and wurtzite are Mn-rich, and were found to contain several trace elements (e.g., Fe, Cu, Se, and Cd) with concentrations greater than 500 ppm and a discernable differentiation between the sphalerite and wurtzite. Noteworthy, 1450 ppm Ga in the wurtzite and 1750 ppm in the sphalerite phases were also reported [8], with estimated standard deviations of 30 and 80 ppm, respectively. In both the sphalerite and wurtzite phases, trace Ga and Cu concentrations were consistent with the coupled substitution $\text{Cu}^+ + \text{Ga}^{3+} \leftrightarrow 2\text{Zn}^{2+}$.

In the course of our ongoing project dealing with the characterization of the Merelani mineralization [2,5–7], we recovered a specimen containing an exceptionally Ga-enriched stannite, with the Ga content indicating a new mineral species. This paper deals with the description of this mineral as new independent species, which was named richardsite. Richardsite is the first gallium-essential sulfide to be described from the Merelani area, joining a very short list of accepted Ga-defined species, of which only three others are sulfides: gallite CuGaS_2 , ishiharaite $(\text{Cu,Ga,Fe,In,Zn})\text{S}$, and zincobriartite $\text{Cu}_2(\text{Zn,Fe})(\text{Ge,Ga})\text{S}_4$.

The new mineral and its name have been approved by the Commission of New Minerals, Nomenclature and Classification of the International Mineralogical Association (No. 2019-136). It is named in honor of Dr. R. Peter Richards (b. 1943), retired water-quality researcher at Heidelberg College (Tiffin, OH, USA) and consulting editor of the journal *Rocks & Minerals*, in recognition of his research and writing, spanning over four decades, on topics related to understanding the genesis of the morphology of minerals. Dr. Richards was a major contributor to the discovery and description of the new minerals carlsonite and huizingite-(Al), and the previously unknown 2H and 3R polytypes of sabieite, all from the Huron River shale fire in Huron County, Ohio, USA [9]. Holotype material is deposited in the collections of the Museo di Storia Naturale, Università degli Studi di Firenze, Via La Pira 4, I-50121, Firenze, Italy, catalogue number 3555/I, and the A. E. Seaman Mineral Museum, 1404 E. Sharon Ave., Houghton, Michigan 49931-1659, USA, catalogue number DM 31876.

2. Occurrence

Richardsite occurs on the faces of a cluster of dark orange-brown wurtzite–sphalerite crystals (to ~2.5 cm across) on a single-known specimen (4.2 cm × 2.6 cm × 1.5 cm) (Figure 1) from the Merelani gem mines. The specimen was obtained in November 2019 through the secondary mineral market, and its precise origin from among the numerous mine workings is unknown. In addition to the primary wurtzite–sphalerite, associated minerals include a second generation of epitaxial sphalerite on the earlier wurtzite–sphalerite, grains of Ge,Ga-rich wurtzite, minor hexagonal graphite crystals, and minor transparent, pale green crystals of diopside. The order of crystallization appears to be (wurtzite–sphalerite)/sphalerite/(richardsite + Ge,Ga-rich wurtzite)/(diopside + graphite).

Numerous studies and reviews are available in the literature on the geology of the Merelani gem deposits and models of formation of the gem crystals, particularly for zoisite (tanzanite) and grossular (tsavorite) (see, for example, [1,4,10–13] and references therein). However, despite the significance of the large sulfide crystals [6] and associated sulfide deposits at the Merelani gem mines, we are not aware of any studies to date of their geological extent, significance, or formation.

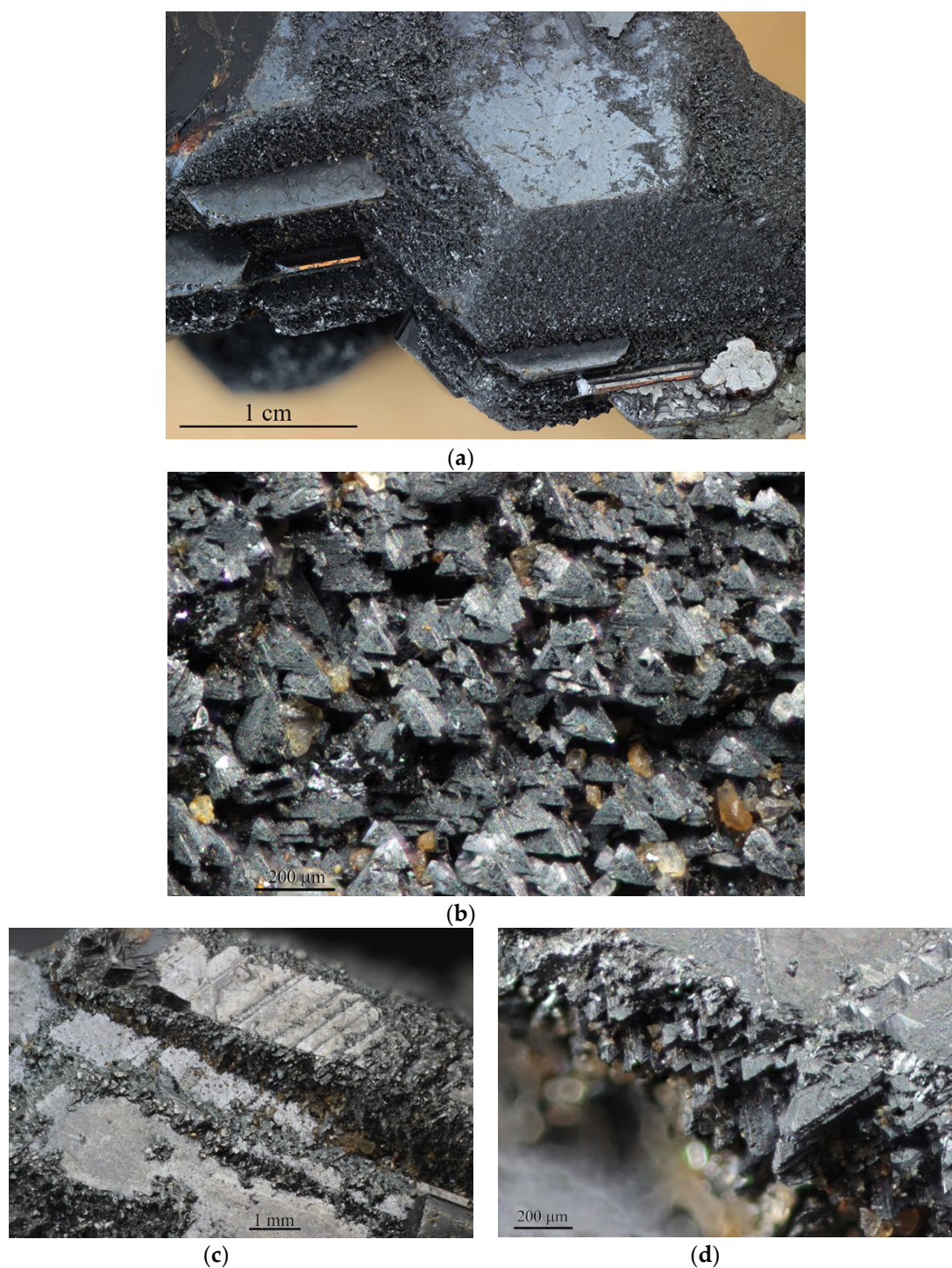


Figure 1. (a) Richardsite coating a wurtzite–sphalerite crystal cluster with oriented terraces of secondary sphalerite crystals (not coated by richardsite). Minor diopside is present at the lower right. (b) Nearly parallel growth of richardsite crystals showing disphenoidal forms with stepped surfaces. (c,d) Apparent epitaxial overgrowth of richardsite on selective facets of primary wurtzite–sphalerite crystals.

3. Analytical Methods

Reflectance values were measured in air using an MPM-200 Zeiss microphotometer (Zeiss, Jena, Germany) equipped with an MSP-20 system processor on a Zeiss Axioplan ore microscope. The filament temperature was approximately 3350 K. An interference filter was adjusted, in turn, to select four wavelengths for measurement (471.1, 548.3, 586.6, and 652.3 nm). Readings were taken for the

specimen and the standard (SiC) maintained under the same focus conditions. The diameter of the circular measuring area was 0.05 mm.

Unpolarized micro-Raman spectra were obtained in nearly back-scattered geometry with a Jobin-Yvon Horiba LabRAM HR800 instrument (HORIBA Jobin Yvon, Edison, NJ, USA) equipped with a motorized x–y stage, an Olympus BX41 microscope (Olympus, Tokyo, Japan) with a 100× objective, polarized incident HeNe laser radiation (632.8 nm), and a neutral density filter (D0.3). Spectra were collected through multiple acquisitions with single counting times of 10 s, and repeated on natural and broken surfaces (not polished) of several crystal grains. No damage from the laser was observed on the samples under these conditions.

Quantitative chemical analyses were carried out using a JEOL 8200 microprobe (JEOL, Akishima, Japan), WDS mode, 20 kV, 20 nA, 1 µm beam size, with counting times of 20 s for peak and 10 s for background). For the WDS analyses, the following lines (standards in parentheses) were used: SKα (sphalerite), FeKα (pyrite), CuKα (synthetic Cu₂S), ZnKα (sphalerite), GaKα (synthetic Ga₂S₃), GeKα (synthetic Ge₂S₃), MnKα (synthetic MnS), and SnLβ (synthetic SnS).

Single-crystal X-ray studies were carried out using a Bruker D8 Venture Photon 100 CMOS (Bruker, Billerica, MA, USA) equipped with graphite-monochromatized MoKα radiation ($\lambda = 0.71073$ Å) operating at 60 kV. The detector-to-crystal distance was 50 mm. Data were collected using ω and φ scan modes, in 0.5° slices, with an exposure time of 45 s per frame. Single-crystal X-ray diffraction intensity data were integrated and corrected using the software package APEX3 (Bruker AXS Inc., Madison, WI, USA, [14]). A total of 955 unique reflections was collected.

X-ray powder diffraction data were collected with a Bruker D8 Venture Photon 100 CMOS using copper radiation (CuKα, $\lambda = 1.54138$ Å). The observed diffraction rings were converted to a conventional powder diffraction pattern using APEX3 [14].

4. Appearance and Physical Properties

Richardsite occurs as overgrowths of small crystals that appear to be epitaxially oriented on the crystal faces of a cluster of wurtzite–sphalerite crystals that is approximately 2.5 cm in maximum dimension (Figure 1). Second-generation sphalerite crystals are crystallographically oriented on the faces of the primary wurtzite–sphalerite. The richardsite appears to selectively occur more richly on some faces of the wurtzite–sphalerite than others, and does not to occur at all on the faces of the second-generation sphalerite. Richardsite crystals exhibit subhedral morphology with pseudo-tetrahedral disphenoidal habit and stepped surfaces. No twinning has been observed. The typical size of richardsite crystals is about 50 to 150 µm, while the maximum size observed is about 400 µm. The physical properties of richardsite are summarized in Table 1.

Table 1. Physical properties of richardsite.

Physical Property	Observation
Color	Dark gray
Streak	Black
Luster	Metallic
Fluorescence	Non-fluorescent
Hardness (Mohs)	3
Hardness (microindentation)	Not measured
Cleavage	None observed
Parting	None observed
Tenacity	Brittle
Fracture	Irregular
Density	Could not be measured due to the small grain size
Density (calculated)	4.278 g·cm ^{−3} using the ideal formula and X-ray single-crystal data
Magnetic properties	Not measured

5. Optical Properties

In reflected plane-polarized light, richardsite appears dark bluish gray in color and is moderately birefractant. Between crossed polarizers, it is distinctly anisotropic with violet to light-blue rotation tints. Richardsite shows neither pleochroism nor internal reflections, and no optical indications of growth zonation are evident. Reflectance data of richardsite at four wavelengths are summarized in Table 2.

Table 2. Reflectance data for richardsite.

R_{\max}	R_{\min}	λ (nm)
25.0	23.5	471.1
28.9	27.4	548.3
29.4	28.1	586.6
28.9	27.7	652.3

6. Raman Spectroscopy

The Raman spectrum of richardsite is shown in Figure 2. The most distinct Raman bands occur at 276, 309, 350, and 366 cm^{-1} , with the peak at 309 cm^{-1} being the narrowest and most intense. Broader and less intense bands occur at 172, 676, and 722 cm^{-1} . The second-most intense peak in most spectra taken is that at 366 cm^{-1} , however, the relative intensities of the 366 and 350 cm^{-1} peaks tend to vary in spectra taken across the crystal grain and can reach the intensity of the 309 cm^{-1} peak in some spectra. Overall, the Raman spectrum of richardsite is similar to that of renierite, $(\text{Cu}^{1+}, \text{Zn})_{11}\text{Fe}_4(\text{Ge}^{4+}, \text{As}^{5+})_2\text{S}_{16}$ (RRUFF ID: 050428 514 nm [15]). The peak at 350 cm^{-1} may be due to the presence of a Ge,Ga-rich Cu–Zn sulfide (also containing Fe, Al, Sn, Mn, and Sn) that is sometimes intermixed with richardsite and has a very intense Raman response at this frequency shift.

Based on factor group analysis, richardsite, as a stannite-group mineral, may be expected to have 14 Raman-active modes [16,17]. The two A_1 -symmetry modes, which involve vibrations of the S atoms, are expected to be the most intense. Definitive symmetry assignments of the Raman peaks would require more detailed experimental studies, such as polarized Raman spectroscopy, checking for resonance effects, and infrared spectroscopy, which are beyond the scope of this paper.

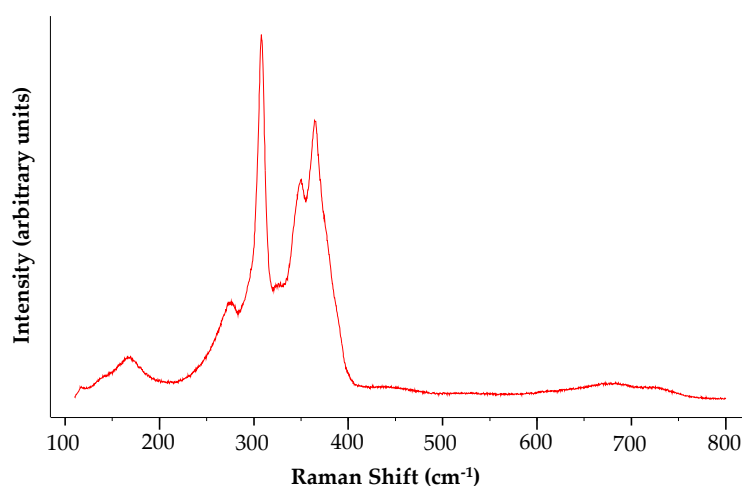


Figure 2. Representative Raman spectrum of a crystalline grain of richardsite in the region 110–800 cm^{-1} using incident laser excitation with a 632.8-nm wavelength.

7. Chemical Composition and X-ray Crystallography

A preliminary chemical analysis using energy-dispersive X-ray spectrometry performed on several crystal fragments, including the one used for the structural study, did not indicate the presence of elements ($Z > 9$) other than Cu, Zn, Ga, S, and minor amounts of Mn, Sn, Fe, and Ge. Subsequent electron microprobe analyses ($n = 4$) revealed the fragment used for the structural study

to be homogeneous within analytical error. Microprobe data are presented in Table 3. Detection limits are <0.01 wt. % for the major elements (Ga, Zn, Cu, S), and <0.02 wt. % for the minor elements (Mn, Sn, Fe, Ge).

Table 3. Electron microprobe data (means and ranges in wt. % of elements) for richardsite.

Constituent	Mean	Range	Standard Deviation (σ)
Mn	0.10	0.07–0.14	0.03
Sn	0.15	0.10–0.21	0.03
Fe	0.41	0.31–0.55	0.04
Ga	17.60	17.22–17.92	0.16
Ge	0.08	0.05–0.12	0.04
Zn	32.85	32.11–33.24	0.22
Cu	16.08	15.68–16.48	0.15
S	32.55	32.08–33.11	0.31
Total	99.81	98.03–101.11	

The empirical formula, based on 8 atoms per formula unit, is: $(\text{Zn}_{1.975}\text{Cu}_{0.995}\text{Ga}_{0.995}\text{Fe}_{0.025}\text{Mn}_{0.010}\text{Ge}_{0.005}\text{Sn}_{0.005})\Sigma 4.010\text{S}_{3.990}$. The simplified formula is $(\text{Zn,Cu})_2(\text{Cu,Fe,Mn})(\text{Ga,Ge,Sn})\text{S}_4$, and the ideal formula is $\text{Zn}_2\text{CuGaS}_4$, which requires Zn 33.34, Cu 16.20, Ga 17.77, and S 32.69, totaling 100 wt. %.

Single-crystal X-ray diffraction indicates that richardsite is tetragonal, with $a = 5.3626(2)$ Å, $c = 10.5873(5)$ Å, $V = 304.46(2)$ Å³, and $Z = 2$. It belongs to space group $I\bar{4}2m$ (#121) and point group $\bar{4}2m$. Least squares refinement of X-ray powder diffraction data (Table 4) give the tetragonal unit cell-parameter values as $a = 5.3622(3)$ Å, $c = 10.5844(10)$ Å, and $V = 304.33(3)$ Å³.

Table 4. Observed and calculated¹ X-ray powder diffraction data (d -spacings in Å) for richardsite. The strongest four estimated relative intensities I are given in bold type.

Miller Indices			Observed		Calculated ¹	
h	k	l	d_{obs}	I_{est}	d_{calc}	I_{calc}
1	1	2	3.084	100	3.0827	100
2	0	0	-	-	2.6813	8
0	0	4	-	-	2.6468	4
2	2	0	1.898	20	1.8960	19
2	0	4	1.882	40	1.8837	36
3	1	2	1.614	20	1.6150	23
1	1	6	1.600	10	1.5998	11
4	0	0	-	-	1.3406	5
3	3	2	-	-	1.2294	4
3	1	6	-	-	1.2227	7
4	2	4	1.092	10	1.0923	9
2	2	8	-	-	1.0852	4
5	1	2	-	-	1.0315	4
5	3	2	-	-	0.9061	3
5	1	6	-	-	0.9034	3
3	1	10	-	-	0.8981	3

¹ Calculated values obtained with the atom coordinates and $\text{Zn}_2\text{CuGaS}_4$ stoichiometry as reported in Table 5 (only reflections with $I_{\text{rel}} \geq 3$ are listed).

The observed tetragonal unit-cell together with the obtained chemical formula suggests that richardsite is a new member of the stannite group. However, two closely related models have been proposed by Hall et al. [18] for the structure of these quaternary chalcogenides, which are topologically equivalent, but differ in the distributions of metals among the positions at $(0,0,0)$, $(0, \frac{1}{2}, \frac{1}{4})$, and $(0, \frac{1}{2}, \frac{3}{4})$ [19]. In particular, the structure of stannite ($\text{Cu}_2\text{FeSnS}_4$) is consistent with the $I\bar{4}2m$ symmetry, having Fe located at the origin ($2a$), Sn located at $2b$ $(0,0, \frac{1}{2})$, and Cu at $4d$ $(0, \frac{1}{2}, \frac{1}{4})$.

In this structure, the Fe and Sn atoms alternate in a chessboard fashion within the layers at $z = 0$ and $\frac{1}{2}$, whereas the layers at $z = \frac{1}{4}$ and $\frac{3}{4}$ have only Cu [20]. The structure of k sterite ($\text{Cu}_2\text{ZnSnS}_4$), on the other hand, has one Cu atom at the $2a$ (0,0,0) position, and Sn located at $2b$ (0,0, $\frac{1}{2}$). Zn and the remaining Cu atom are ordered at $2c$ (0, $\frac{1}{2}$, $\frac{1}{4}$) and $2d$ ($\frac{1}{2}$,0, $\frac{1}{4}$) [equivalent to (0, $\frac{1}{2}$, $\frac{3}{4}$)] positions, respectively. This leads to both the Cu,Sn layers (at $z = 0$ and $\frac{1}{2}$) and the Zn,Cu layers (at $z = \frac{1}{4}$ and $\frac{3}{4}$) having the metal atoms alternating in a chessboard fashion [20]. With different atoms occupying the $2c$ and $2d$ positions in k sterite, the mirror plane parallel to (110) is lost, giving a structure with space group $I\bar{4}$. In both structural models, S lies on the (110) mirror plane at $8i$ (x,x,z) for stannite, or on the general position $8g$ (x,y,z) for k sterite.

In order to determine the distribution of metal atoms in richardsite without symmetry constraints, the structure was refined in both space groups, and better agreement was obtained in $I\bar{4}2m$. The crystal structure was refined using the program SHELXL-97 [21] up to $R1 = 0.0284$ for 655 reflections with $F_o > 4\sigma(F_o)$ and 14 parameters. The refined mean electron number at the metal sites, using scattering curves for neutral atoms taken from the *International Tables for Crystallography* [22], was 30 (Wyckoff position $4d$), 31 ($2a$), and 29 ($2b$); thus, given also the observed mean bond distances and the chemical data, Zn, Ga, and Cu were assigned, respectively, to the three tetrahedral sites. Of course, due to the iso-electronic nature of its constituent elements ($\text{Cu} = 29$, $\text{Zn} = 30$, $\text{Ga} = 31$) together with the ambiguity in their valence states, the metal partitioning in richardsite is, however, not straightforward. According to Brese and O’Keeffe [23], the ideal distance (in  ) in a regular tetrahedron decreases following the sequence: 2.370/ Cu^+ , 2.346/ Zn^{2+} , 2.288/ Ga^{3+} , 2.116/ Cu^{2+} , and this distribution is in keeping with the site-assignment proposed here for richardsite (Table 6). Furthermore, the chemical data clearly point to a new mineral species, regardless of the site distribution. Final atomic coordinates and equivalent isotropic displacement parameters are given in Table 5, and selected metal-sulfur (Me-S) bond distances are shown in Table 6. The Crystallographic Information File (CIF) is available as Supplementary Material.

Table 5. Atoms, Wyckoff positions, atom coordinates, and isotropic displacement parameters (U_{iso} in  ²) for richardsite.

Atom	Wyckoff	x/a	y/b	z/c	U_{iso}
Zn	$4d$	0	$\frac{1}{2}$	$\frac{1}{4}$	0.01187(13)
Ga	$2a$	0	0	0	0.00993(13)
Cu	$2b$	0	0	$\frac{1}{2}$	0.02108(12)
S	$8i$	0.75389(6)	0.75389(6)	0.87356(4)	0.01009(11)

Table 6. Me-S bond distances for richardsite.

Bond Type	Bond Distance (�)
Cu-S	2.3451(5) (�4)
Zn-S	2.3037(3) (�4)
Ga-S	2.2969(5) (�4)

The structure of richardsite consists of a cubic close packing (*ccp*) array of sulfur atoms tetrahedrally bonded with metal atoms occupying one half of the *ccp* tetrahedral voids (Figure 3). The ordering of the metal atoms leads to a sphalerite(sph)-derivative tetragonal unit-cell, with $a \approx a_{\text{sph}}$ and $c \approx 2a_{\text{sph}}$. The packing of the S atoms slightly deviates from the ideal, however, primarily due to the presence of Ga.

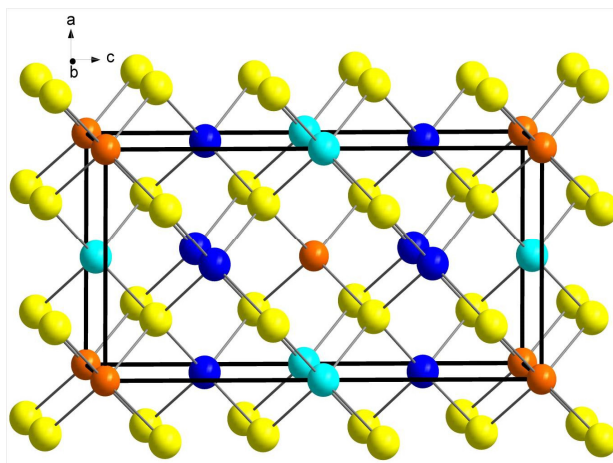


Figure 3. The crystal structure of richardsite. Cu, Zn, Ga, and S atoms are given as light blue, dark blue, orange, and yellow circles, respectively. The unit cell of the structure is outlined in black, and its orientation is indicated at the top left.

8. Discussion

Minerals of the stannite group are quaternary chalcogenides, typically with the general formula $T_1T_2T_3X_4$, where T1, T2, and T3 correspond to tetrahedrally coordinated cations, and X corresponds to monatomic anions [24]. Among the mineral species, including richardsite, accepted by the Commission of New Minerals, Nomenclature and Classification of the International Mineralogical Association, T1 = Ag, Cu, Zn; T2 = Ag, Cu, Cd, Fe, Hg, Zn; T3 = As, Ga, Ge, In, Sb, Sn; and X = S, Se. Group members are generally tetragonal but can also be orthorhombic, and their structures can be considered derivatives of the sphalerite (or chalcopyrite) structure type [20,25], with the types of cations and their ordering in the tetrahedral sites affecting the resulting overall symmetry of the structures.

Richardsite is the Ga-analogue of UM1985-23-S:CuFeInZn ($CuZn_2InS_4$) described by Cantinolle et al. [26] and by Kieft and Damman [27] as the end-member of the k esterite–sakuraiite series. A similar phase to UM1985-23-S:CuFeInZn (same stoichiometry) but possibly with the sphalerite-type structure, has been reported by Ohta [28] and Semenyak et al. [29].

A wide variety of ternary (I–III–VI₂) and quaternary (I₂–II–IV–VI₄) chalcogenides (I = Cu, Ag; II = Zn, Cd, Mn; III = Al, Ga, In; IV = Ge, Sn; VI = S, Se, Te) have been the subject of recent interest for their potential applications in photovoltaic devices, thermoelectric devices, and solar energy conversion materials [30]. The difficulty of distinguishing between the kesterite and stannite structures, particularly with the high potential for (Cu + Zn) disorder, has been noted for the (Cu,Zn)-containing quaternary phases (see [30] and references therein). Quaternary chalcogenides containing Ga do not appear to have been synthesized until more recently, as in a study of wurtzite and stannite phases of Cu_2ZnAS_{4-x} and $CuZn_2AS_4$ (A = Al, Ga, In) nanocrystals [31]. These nanocrystals were synthesized using the colloidal hot-injection method as disordered-wurtzite phases. Upon annealing for 2–2.5 h in an N₂ atmosphere at temperatures of 400–450 °C for Cu_2ZnAS_{4-x} and 500 °C for $CuZn_2AS_4$, the nanocrystals transformed to ordered stannite phases. Single-crystal X-ray studies and structure refinements have not been carried out on these synthetic materials, however.

First-principles calculations for both Cu_2ZnAS_{4-x} [31] and $CuZn_2AS_4$ [31,32] materials indicate that they are direct band gap materials with high absorption coefficients for visible light and, as such, they show initial promise as radiation-absorbing materials for solar cells. First-principles calculations [32] also show the $CuZn_2AS_4$ materials to be *p*-type semiconductors, and that the stannite-type structure is energetically more stable than the kesterite- and wurtzite-type structures.

Supplementary Materials: The following are available online at www.mdpi.com/2075-163X/10/5/467/s1, CIF File S1: richardsite.

Author Contributions: J.A.J. recognized the potential uniqueness of the specimen and performed the initial SEM-EDS and Raman studies. L.B. performed the X-ray diffraction experiments and analysis, electron microprobe analyses, and reflectivity measurements. Both authors wrote the manuscript and have read and agreed to the published version of the manuscript. All authors have read and agreed to the published version of the manuscript.

Funding: Analytical work performed at Michigan Technological University's Applied Chemical and Morphological Analysis Laboratory was supported in part by the Edith Dunn and E. W. Heinrich Mineralogical Research Trust. The research was also funded by MIUR-PRIN2017, project "TEOREM deciphering geological processes using Terrestrial and Extraterrestrial ORE Minerals", prot. 2017AK8C32 (PI: Luca Bindi).

Acknowledgments: J.A.J. thanks Y.K. Yap at Michigan Technological University for use of the Raman spectrometer in his laboratory.

Conflicts of Interest: The authors declare no conflict of interest.

References

1. Wilson, W.E.; Saul, J.M.; Pardieu, V.; Hughes, R.W. The Merelani tanzanite mines, Lelatema Mountains, Arusha Region, Tanzania. *Mineral. Rec.* **2009**, *40*, 347–408.
2. Jaszczak, J.A.; Trinchillo, D. Miracle at Merelani: A remarkable occurrence of graphite, diopside, and associated minerals from the Karo mine, Block D, Merelani Hills, Arusha region, Tanzania. *Rocks Miner.* **2013**, *88*, 154–165, doi:10.1080/00357529.2013.763671.
3. Long, J.M.; Rakovan, J.; Jaszczak, J.A.; Sommer, A.J.; Anczkiewicz, R. Fluorapatite from a remarkable occurrence of graphite and associated minerals. *Rocks Miner.* **2013**, *88*, 178–183, doi:10.1080/00357529.2013.763690.
4. Giuliani, G.; (Ed.) *Les Gemmes du Gondwana; Les Cahiers du Règne Minéral No. 2*; Editions du Piat: Saint-Julien-du-Pinet, France, 2013; 146p.
5. Weiss, S.; Jaszczak, J.A.; Harrison, S.; Hintze, J.; Radl, W. Merelani: Tansanit und seltene Sammlermineralien. *Lapis* **2015**, *40*, 34–63.
6. Harrison, S.; Jaszczak, J.A.; Keim, M.; Rumsey, M.; Wise, M.A. Spectacular sulfides from the Merelani tanzanite deposit, Manyara Region, Tanzania. *Mineral. Rec.* **2014**, *45*, 553–570.
7. Jaszczak, J.A.; Rumsey, M.S.; Bindi, L.; Hackney, S.A.; Wise, M.A.; Stanley, C.J.; Spratt, J. Merelaniite, $\text{Mo}_4\text{Pb}_4\text{VSbS}_{15}$, a new molybdenum-essential member of the cylindrite group, from the Merelani tanzanite deposit, Lelatema Mountains, Manyara region, Tanzania. *Minerals* **2016**, *6*, 115, doi:10.3390/min6040115.
8. Pring, A.; Wade, B.; McFadden, A.; Lenehan, C.E.; Cook, N.J. Coupled substitutions of minor and trace elements in co-existing sphalerite and wurtzite. *Minerals* **2020**, *10*, 147, doi:10.3390/min10020147.
9. Richards, R.P.; Shewfelt, W.R.; Carlson, E.H.; Kampf, A.R.; Nash, B.P. Mineralogy of the Huron River Shale Fire, Huron County, Ohio. *Rocks Miner.* **2017**, *92*, 244–263, doi:10.1080/00357529.2017.1283660.
10. Weiss, S. Edelsteinbergbau in Merelani, Tansania. *Lapis* **2015**, *40*, 12–33.
11. Olivier, B. The Geology and Petrology of the Merelani Tanzanite Deposit, Tanzania. Ph.D. Thesis, University of Stellenbosch, Stellenbosch, South Africa, 2006. Available online: <https://scholar.sun.ac.za/bitstream/handle/10019.1/1093/olivier-b-2008.pdf> (accessed on 9 April 2020).
12. Harris, C.; Hlongwane, W.; Gule, N.; Scheepers, R. Origin of tanzanite and associated gemstone mineralization at Merelani, Tanzania. *South Afr. J. Geol.* **2014**, *117*, 15–30.
13. Feneyrol, J.; Giuliani, G.; Ohnenstetter, D.; Fallick, A.E.; Martelat, J.E.; Monié, P.; Dubessy, J.; Rollion-Bard, C.; Le Goff, E.; Malisa, A.; et al. New aspects and perspectives on tsavorite deposits. *Ore Geol. Rev.* **2013**, *53*, 1–25.
14. Bruker. APEX3; Bruker AXS Inc.: Madison, WI, USA, 2016. Available online: <https://www.bruker.com/products/x-ray-diffraction-and-elemental-analysis/single-crystal-x-ray-diffraction/sc-xrd-software/apex3.html> (accessed on 12 April 2020).
15. Lafuente, B.; Downs, R.T.; Yang, H.; Stone, N. The power of databases: The RRUFF project. In *Highlights in Mineralogical Crystallography*; Armbruster, T., Danisi, R.M., Eds.; W. De Gruyter: Berlin, Germany, 2015; pp. 1–30.
16. Fontané, X.; Izquierdo-Roca, V.; Saucedo, E.; Schorr, S.; Yukhymchuk, V.O.; Valakh, M.Ya.; Pérez-Rodríguez, A.; Morante, J.R. Vibrational properties of stannite and kesterite type compounds: Raman scattering analysis of $\text{Cu}_2(\text{Fe,Zn})\text{SnS}_4$. *J. Alloy. Compds.* **2012**, *539*, 190–194, doi:10.1016/j.jallcom.2012.06.042.

17. Rincón, C.; Quintero, M.; Moreno, E.; Power, Ch.; Quintero, E.; Henao, J.A.; Macías, M.A. Raman spectrum of $\text{Cu}_2\text{CdSnSe}_4$ stannite structure semiconductor compounds. *Superlatt. Microstruct.* **2015**, *88*, 99–103, doi:10.1016/j.spmi.2015.08.032.
18. Hall, S.R.; Szymanski, J.T.; Stewart, J.M. Kesterite, $\text{Cu}_2(\text{Zn,Fe})\text{SnS}_4$, and stannite, $\text{Cu}_2(\text{Fe,Zn})\text{SnS}_4$, structurally similar but distinct minerals. *Can. Miner.* **1978**, *16*, 131–137.
19. Bonazzi, P.; Bindi, L.; Bernardini, G.P.; Menchetti, S. A model for the mechanism of incorporation of Cu, Fe, and Zn in the stannite–kesterite series, $\text{Cu}_2\text{FeSnS}_4$ – $\text{Cu}_2\text{ZnSnS}_4$. *Can. Miner.* **2003**, *41*, 639–647.
20. Makovikcy, E. Crystal structures of sulfides and other chalcogenides. *Rev. Miner. Geochem.* **2006**, *61*, 7–125.
21. Sheldrick, G.M. A short history of SHELX. *Acta Crystallogr.* **2008**, *64*, 112–122, doi:10.1107/S0108767307043930.
22. Wilson, A.J.C. *International Tables for Crystallography: Mathematical, Physical, and Chemical Tables*, International Union of Crystallography: Chester, UK, 1992; Volume 3.
23. Brese, N.E.; O’Keeffe, M. Bond-valence parameters for solids. *Acta Cryst.* **1991**, *47*, 192–197.
24. Nickel, E.H. Discussion Paper on Mineral Groups. Available online: <https://www.ima-mineralogy.org/docs/Nickel.pdf> (accessed on 10 May 2020).
25. Vaughan, D.J.; Corkhill, C.L. Mineralogy of Sulfides. *Elements* **2017**, *13*, 81–87, doi:10.2113/gselements.13.2.81.
26. Cantinolle, P.; Laforêt, C.; Maurel, C.; Picot, P.; Grangeon, J. Contribution to the mineralogy of indium: Discovery of two new indium sulfides and of two new occurrences of roquesite in France. *Bull. De Minéralogie* **1985**, *108*, 245–248. (In French)
27. Kieft, K.; Damman, A.H. Indium-bearing chalcopyrite and sphalerite from the Gåsborn area, West Bergslagen, central Sweden. *Miner. Mag.* **1990**, *54*, 109–112.
28. Ohta, E. Occurrence and chemistry of indium-containing minerals from the Toyoha mine, Hokkaido, Japan. *Min. Geol.* **1989**, *39*, 355–372.
29. Semenyak, B.I.; Nedashkovskii, A.P.; Nikulin, N.N. Indium minerals in the ores of the Pravourmiiskoe deposit (Russian Far East). *Geol. Ore Depos.* **1994**, *36*, 207–213.
30. Fan, F.-J.; Wu, L.; Yu, S.-H. Energetic I-III-VI₂ and I₂-II-IV-VI₄ nanocrystals: Synthesis, photovoltaic and thermoelectric applications. *Energy Env. Sci.* **2014**, *7*, 190–208, doi:10.1039/c3ee41437j.
31. Ghosh, A.; Palchoudhury, S.; Thangavel, R.; Zhou, Z.; Naghibolashrafi, N.; Ramasamy, K.; Gupta, A. A new family of wurtzite-phase $\text{Cu}_2\text{ZnAS}_{4-x}$ and CuZn_2AS_4 (A = Al, Ga, In) nanocrystals for solar energy conversion applications. *Chem. Commun.* **2016**, *52*, 264–267, doi:10.1039/c5cc07743e.
32. Yalcin, B.G. Thermoelectric properties of stannite-phase CuZn_2AS_4 (CZAS; A = Al, Ga and In) nanocrystals for solar energy conversion applications. *Philos. Mag.* **2016**, *96*, 2280–2299, doi:10.1080/14786435.2016.1197433.

